lubricants

MDPI

Article

Study on Distribution of Lubricating Oil Film in Contact Micro-Zone of Full Ceramic Ball Bearings and the Influence Mechanism on Service Performance

Jinmei Yao [1], Yuhou Wu [1], Jiaxing Yang [1], Jian Sun [1,2,*], Zhongxian Xia [1], Junxing Tian [1], Zhigang Bao [1] and Longfei Gao [1]

[1] School of Mechanical Engineering, Shenyang Jianzhu University, Shenyang 110168, China; yaojinmei06@126.com (J.Y.); wuyh@sjzu.edu.cn (Y.W.); a18946295255@163.com (J.Y.); xiazx17@sjzu.edu.cn (Z.X.); tianjunxingge@163.com (J.T.); bzg0123@126.com (Z.B.); gaolongfei005@126.com (L.G.)
[2] School of Mechanical Engineering, Tsinghua University, Beijing 100084, China
* Correspondence: sunjian@sjzu.edu.cn

Abstract: Compared with metal ball bearings, full ceramic ball bearings have more outstanding service performance under extreme working conditions. In order to reveal the lubrication mechanism and improve the operation performance and service life of full ceramic ball bearings, in this paper, the friction, vibration, and temperature rise characteristics of 6208 silicon nitride full ceramic deep groove ball bearing, under the condition of oil lubrication, are studied experimentally. Based on the test results, and through theoretical calculation and simulation analysis, the distribution of the lubricating oil film in bearing contact micro-zone under different working conditions was simulated. After that, the surface of contact micro-zone of full ceramic ball bearing was analyzed. It was found that there is an optimal oil supply for full ceramic ball bearing oil lubrication in service. Under the optimal oil supply lubrication, full film lubrication can be achieved, and the bearing exhibits the best characteristics of friction, vibration, and temperature rise. Compared with the load, the rotational speed of the bearing has a decisive influence on the optimal oil supply. When the rotational speed and load are constant, the minimum oil film thickness and oil film pressure in the contact area of the rolling body decrease with the increase of angle ψ from the minimum stress point of the rolling body. Under the action of high contact stress, thin oil film will be formed in the bearing outer ring raceway. In the field of full ceramic ball bearings, the research content of this paper is innovative. The research results of this paper have an important guiding significance for revealing the oil lubrication mechanism of full ceramic ball bearing and enriching its lubrication theory and methods.

Keywords: full ceramic ball bearing; lubricant oil film; service performance; simulation model

Citation: Yao, J.; Wu, Y.; Yang, J.; Sun, J.; Xia, Z.; Tian, J.; Bao, Z.; Gao, L. Study on Distribution of Lubricating Oil Film in Contact Micro-Zone of Full Ceramic Ball Bearings and the Influence Mechanism on Service Performance. *Lubricants* **2022**, *10*, 174. https://doi.org/10.3390/lubricants10080174

Received: 29 May 2022
Accepted: 26 July 2022
Published: 1 August 2022

1. Introduction

Full ceramic ball bearings refer to high-tech bearing products whose rings and rolling bodies are made of ceramic materials. It has excellent performance at high speed, compression resistance, high/low temperature resistance, wear resistance, corrosion resistance, and electromagnetic insulation, as well as other aspects, and can be widely used in aerospace, navigation, metallurgy, chemical and national defense, and military fields [1–3]. A good lubrication state is the prerequisite for the normal operation of full ceramic ball bearings. It is also an important factor affecting the performance of the bearings, such as friction, vibration, and temperature rise under complex working conditions [4]. At present, based on the lubrication theory of metal ball bearing, experts and scholars at home and abroad have carried out relevant research on the operation performance of ceramic ball bearings under oil lubrication conditions.

Meyer L. D [5] studied the analytical method for the continuous and periodic changes of the ball contact force when the bearing rotates, based on the Lagrange equation for solving time-varying displacement of the bearing. N. Lynagh [6] established a detailed bearing vibration model by considering the influence of rolling body surface corrugation and ball size on radial clearance and deduced the vibration force and torque generated by bearing movement by using the formula. It provides a great reference for the subsequent research. Mohammed Alfares [7] studied the influence of heat generation on the performance of ball bearings during service, as well as the influence of this heat effect on system dynamics, by using transient thermal model. A set of differential equations was obtained by using thermal equilibrium. Jalali-vahid D. [8] studied and obtained the multi-stage multi-grid solution for isothermal elastohydrodynamic circular contact problem. By deploying a large number of units, the accuracy of the numerical solution is improved. The conclusion presented in this paper is of great prospective significance and has guiding value for the analysis of isothermal elastic hydrodynamics. As a pioneer in this field, Dowson D. [9] conducted a numerical evaluation on the analysis of point contact of isothermal elastohydrodynamic lubrication. In the elastic analysis, the contact area is divided into equal rectangular areas, and it is assumed that a uniform pressure is applied to each element to analyze the oil film thickness. This paper also carries out a more detailed study on this basis. Ioannides, E. [10] put forward an idea a long time ago to study an analytical model for predicting the life of rolling bearings under the consideration of the fatigue life, fatigue criterion, and fatigue limit of bearings. The viewpoints proposed at that time were forward-looking and provided great significance for the research of bearing field. Zhu Weibing [11] established a calculation model of oil injection lubrication and under-race lubrication for angular contact ball bearings. The results showed that: when the speed and load were low, it was more appropriate to use oil injection lubrication. When the speed and load are high, it is more advantageous to use under-race lubrication. Nagare [12] experimentally analyzed and investigated the effects of performance parameters, such as speed, eccentricity, load, and friction torque, on the performance of overloaded low speed bearings. Liming Lu [13] designed a set of independent devices to explore the impact of impact load on the lubrication performance of roller sliding bearings. The results showed that: the greater the impact load frequency, the greater the minimum oil film thickness, greater the impact load amplitude, and thinner the roller oil film thickness. The sliding of the rolling element may lead to the failure of the rolling bearing. Kang Jianxiong [14] considered the interaction between the ball and raceway, interaction between the cage and raceway, and elastohydrodynamic lubrication and other factors, in order to effectively analyze the sliding characteristics of the rolling bearing using the dynamic response. Antonio [15] studied the influence of lubricant film thickness on bearing service performance under hydrodynamic lubrication conditions. Cho [16] improved the Elrod algorithm based on the mass conservation boundary conditions and obtained the governing equation and the lubrication equation of the complete oil film region that can automatically determine the dynamic boundary. Biswas [17] studied the lubrication performance of medium-low speed bearings under different load conditions, as well as the changes regarding oil film thickness, oil film pressure, and oil film velocity. Dmitrichenko [18] established the dynamic model of ball bearings and studied the influence of different distribution models of lubricants and fluid dynamic pressure on the dynamic characteristics of bearings. Brizmer [19] studied the mechanism of micro-pitting resistance of hybrid ceramic bearings under reduced lubrication conditions, thus providing a new idea for tribology and performance of silicon nitride ceramic rolling bearings. Kang Li [20] analyzed the tribological properties of GCr15-GCr15/Si3N4-GCr15 materials under the condition of oil lubrication by using pin-disc friction and wear testing machine. Xiang Guo [21] studied and investigated the dynamic mixed elastohydrodynamic lubrication behavior of water-lubricated bearings with unbalanced rotors in the starting process.

From the above, it can be seen that most studies were based on metal ball bearings, only part of the research is suitable for the hybrid ceramic ball bearing. Additionally, a

small number of reports on the lubrication mechanism and method of full ceramic ball bearings are only described for the objective phenomena in the lubrication process. The objective laws and scientific problems behind it have not been further revealed. Therefore, this paper takes silicon nitride full ceramic ball bearing as the research object and studies its service performance, regarding friction, vibration, and temperature rise under the condition of oil lubrication. The effects of lubrication, rotational speed, and load on the performance of full ceramic ball bearings were revealed by means of experiments, and the optimal oil supply was determined. Based on the optimal oil supply, the distribution characteristics of lubricating oil film and its influence on service performance of full ceramic ball bearings were revealed by means of calculation and simulation. Finally, the surface characteristics of contact microzone after service of full ceramic ball bearing under oil lubrication condition were analyzed. The research results have important guiding significance for forming a lubrication theory and method suitable for full ceramic ball bearing, as well as improving its service performance and life.

2. Experimental Study on Oil Lubrication Characteristics of Full Ceramic Ball Bearing

2.1. Test Bearings and Components

The test took 6208 silicon nitride full ceramic deep groove ball bearing with P4 accuracy as the research object, carried out the service performance test under oil lubrication condition, and revealed the distribution law of the full ceramic ball bearing lubricating oil film, as well as its influence mechanism on friction performance. The structure of the test bearing is shown in Figure 1. The clearance of the test bearing was C_N standard clearance, and the cage guide mode was an outer ring guide. The lubricating oil used in the test was principal axis oil, with a viscosity value of 30 mm^2/s. The material used for the inner and outer rings and rolling bodies was silicon nitride ceramic, and the powder was produced by Ube Group in Japan and formed by hot isostatic pressing sintering process. The material performance test results are shown in Table 1. The structural parameters of the test bearing are shown in Table 2.

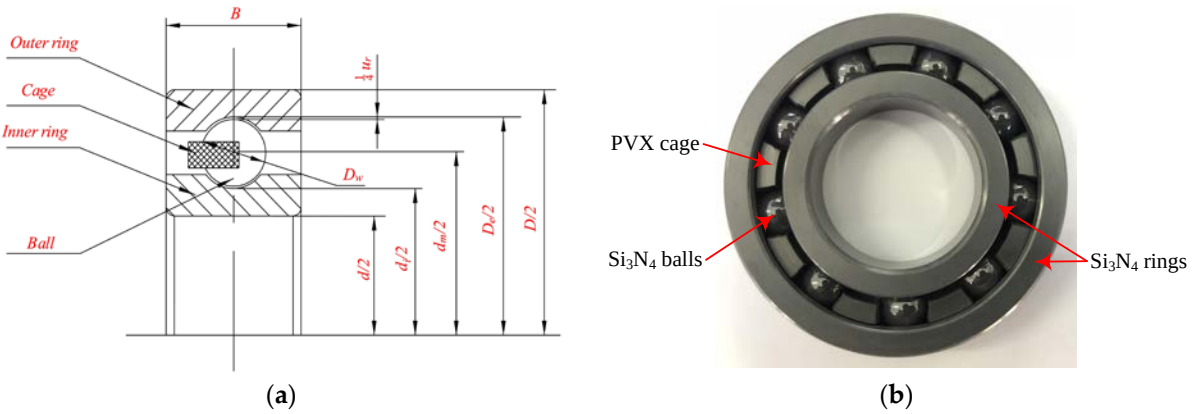

Figure 1. Full ceramic ball bearing for test. (**a**) Structure diagram (**b**) Test bearing diagram.

Table 1. Physical properties of Si_3N_4 for full ceramic ball bearings.

Elastic Modulus (Gpa)	Poisson Ratio	Density (g/cm^3)	Thermal Expansion Coefficient ($10^{-6}/K$)	Thermal Conductivity ($W/m*K$)	Hardness (kg/mm^2)
300–320	0.26	3.2–3.3	3.1–3.5	20–29	1520–1800

Table 2. Structure parameters of 6208 full ceramic ball bearings.

Structure Parameters	Values
Inner diameter d/mm	40
Outer diameter D/mm	80
Pitch diameter d_m/mm	60
Bearing width B/mm	18
Diameter of ball D_w/mm	12
Raceway radius of inner ring r_i/mm	6.17
Raceway radius of outer ring r_e/mm	6.29
Number of rolling elements z	9

The test bearing cage material was carbon dairy produce, PTFE, graphite reinforced PVX-based composite material, which was produced by Ensinger Group in Berlin, Germany. The specific properties of the material are shown in Table 3. The experimental verification and application experience show that the material can be applied to the wide temperature range of −70–200 °C. In addition, the material has the appropriate strength and toughness to withstand a certain load and impact, small friction coefficient, and good wear resistance. It also has smaller specific gravity and similar expansion coefficient to the rolling body, which is suitable for the test project.

Table 3. PVX composite enhanced cage material properties.

Material Properties	Values
Modulus of elasticity/MPa	5500–6000
Tensile strength/MPa	84
Flexural strength/MPa	142
Compression strength/MPa	22–102
Compression modulus/MPa	4000
Impact strength/kJm^{-2}	28
Ball indentation hardness/MPa	250
Glass transition temperature/°C	146
Service temperature/°C	+260–−200
Thermal expansion/10^{-5} K^{-1}	3–4
Specific heat/J/(g·K)	1.1
Thermal conductivity/W/(K·m)	0.82

2.2. Introduction to the Test Equipment

Figure 2 shows the JH-200E rolling bearing testing machine (Shenyang Jianzhu University, Shenyang, China) and its structure. The testing machine is a horizontal bearing performance life testing machine, which is mainly composed of bearing test chamber, axial loading system, radial loading system, test shafting, oil supply system, force sensor, temperature sensor, vibration sensor, and control system. The main test parameters were: the outer diameter of the test bearing was 30–200 mm, the inner diameter was 10–170 mm, and the width was 10–30 mm. Oil supply system flow range: 0.001–10 mL/min, and flow control accuracy was ±0.001 mL/min. The radial loading range of test bearings was 100–30,000 N, and the axial loading range was 50–10,000 N. The maximum spindle rotational speed was 30,000 r/min.

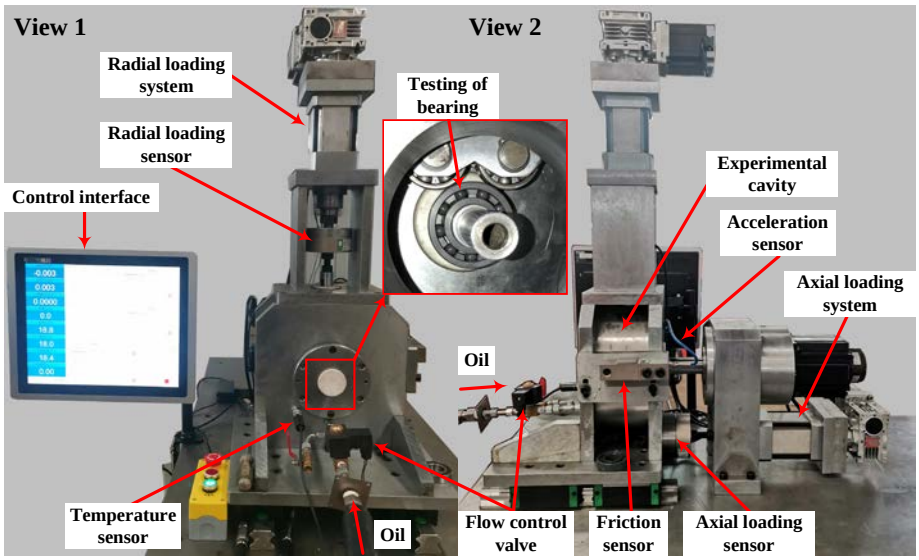

Figure 2. Lubrication test of full ceramic ball bearing oil based on JH-200E (Shenyang Jianzhu University, Shenyang, China).

2.3. Test Scheme Design

The oil lubrication test of the full ceramic ball bearing was carried out at room temperature. The target value is measured by changing the bearing oil supply, bearing radial load, bearing rotational speed, and other working conditions. The specific experimental process was as follows. (1) Before the bearing was started, oil was supplied to the test bearing according to the target set value. (2) Under no-load condition, the test bearing speed was increased from 0 r/min to the set value of the target speed within 3 min. (3) After the oil supply and speed of the test bearing were stable, the radial loading of the test bearing was carried out according to the set value of the target load. (4) After the test lasted for 30 min and the temperature of the test chamber and outer ring of the bearing, vibration value of the bearing, friction value, and other target measurement values were stable, the measurement and recording data were started. The test scheme is shown in Table 4.

Table 4. The 6208 full ceramic ball bearing oil lubrication test scheme.

Serial Number	Radial Load	Contact Stress		Other Index Parameters
		Inner Raceway	Outer Raceway	
1	400 N	1.65 Gpa	1.54 Gpa	Axial load: 0 N Test rotation speed: 5000/10,000 rpm Oil supply: 0.2–2.0 mL/min
2	900 N	2.16 Gpa	2.02 Gpa	
3	1750 N	2.70 Gpa	2.52 Gpa	
4	3000 N	3.23 Gpa	3.01 Gpa	

3. Test Results and Analysis

3.1. Variation Characteristics of Friction

The JH-200E rolling bearing testing machine was used to carry out the full ceramic ball bearing oil lubrication test. Based on the friction sensor, the friction change of the full ceramic ball bearing under variable working conditions was measured, as shown in Figure 3.

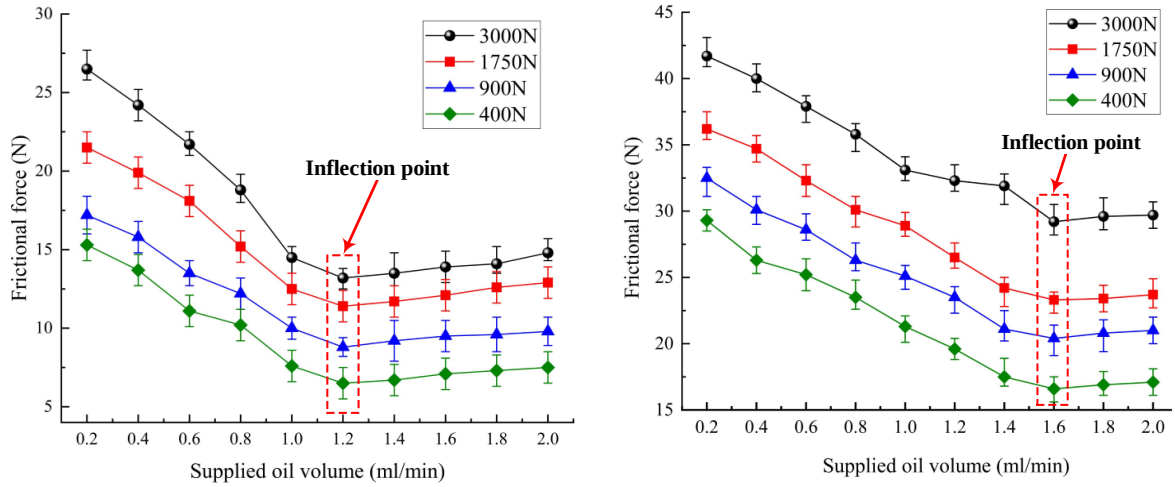

Figure 3. Variation law of friction of full ceramic ball bearing under oil lubrication condition. (**a**) n = 5000 r/min, (**b**) n = 10,000 r/min.

It can be seen from Figure 3 that, when the rotational speed is constant with the increase of oil supply, the friction value of the full ceramic ball bearing decreases first and then increases. When the bearing speed was 5000 r/min, the friction force had a minimum inflection point value in the range of 0.2–2.0 mL/min oil supply, and the value was about 1.2 mL/min oil supply. This indicates that in this particular working condition, when the oil supply was 1.2 mL/min, the full ceramic ball bearing showed the best friction characteristics. When the oil supply was less than 1.2 mL/min, the full ceramic ball bearing was in the state of lack of oil lubrication, and the lubricating oil in the bearing contact micro-zone had not formed the state of full film lubrication, so the friction force was large. In this range, with the continuous increase of oil supply, the lubrication state improved, lubricating oil film gradually thickened, friction decreased, and change trend was very obvious. When the oil supply was greater than 1.2 mL/min, due to the large amount of lubricating oil, the excess lubricating oil produced viscous resistance to the operation of the bearing under the action of viscosity, thus leading to the gradual increase of the friction of the bearing. However, the influence of oil viscosity resistance on the change of friction was relatively small, so when the oil supply was greater than the optimal oil supply, and with the continuous increase of oil supply, the increase trend of friction was relatively moderate. By comparing Figure 3a,b, it can be seen that the oil supply at the inflection point of friction of the full ceramic ball bearings increased gradually with the increase of rotational speed. The change of load had no obvious effect on the oil supply at the inflection point of friction.

3.2. Variation Characteristics of Vibration Acceleration

The JH-200E rolling bearing testing machine was used to carry out the full ceramic ball bearing oil lubrication test, and the vibration variation of the full ceramic ball bearing outer ring under variable working conditions was measured based on the acceleration sensor, as shown in Figure 4.

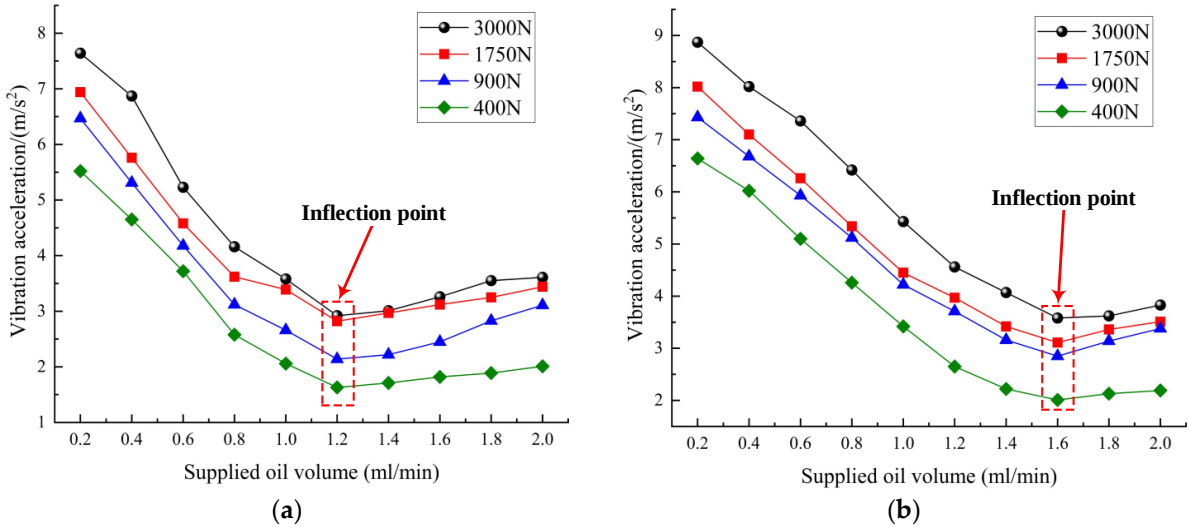

Figure 4. Vibration law of outer ring of full ceramic ball bearing under oil lubrication condition. (**a**) n = 5000 r/min, (**b**) n = 10,000 r/min.

According to Figure 4, when the rotational speed was constant, the vibration acceleration value of the outer ring of the full ceramic ball bearing decreased from large to small and then increased with the increase of oil supply. When the rotational speed was 5000 r/min, the vibration acceleration of outer ring had a minimum inflection point value, and the corresponding oil supply was also about 1.2 mL/min. This indicates that, when the rotational speed was 5000 r/min, the full ceramic ball bearing exhibited the best friction and vibration characteristics under the condition of 1.2 mL/min oil supply, which can be determined as its optimal oil supply. When the oil supply was less than the optimal oil supply, due to the influence of lack of oil lubrication, there was oil–solid mixed lubrication in the bearing contact micro-zone; the sliding roll ratio changed more frequently, and the vibration acceleration value of the bearing outer ring increased accordingly [22–24]. With the continuous increase of oil supply, the lubrication state improved; the vibration value of the bearing's outer ring decreased, and the change trend was very obvious. When the oil supply was greater than the optimal oil supply, the amount of lubricating oil was large, and the excess lubricating oil produced viscous resistance to the operation of the bearing under the action of viscosity, thus leading to a gradual increase in the vibration value of the bearing's outer ring, this phenomenon could be seen in Figure 4. However, the influence of oil viscosity resistance on the vibration change of the bearing's outer ring was relatively small, so when the oil supply was greater than the optimal oil supply, and with the continuous increase of oil supply, the increase trend of vibration acceleration value was relatively moderate [25,26]. In addition, when the radial load of the bearing increased, the vibration acceleration value of the bearing increased accordingly.

3.3. Variation Characteristics of Outer Ring Temperature Rise

The JH-200E rolling bearing testing machine was used to carry out the oil lubrication test of the full ceramic ball bearing, and the temperature rise change of the outer ring of the full ceramic ball bearing is shown in Figure 5, based on the temperature sensor measured under variable working conditions.

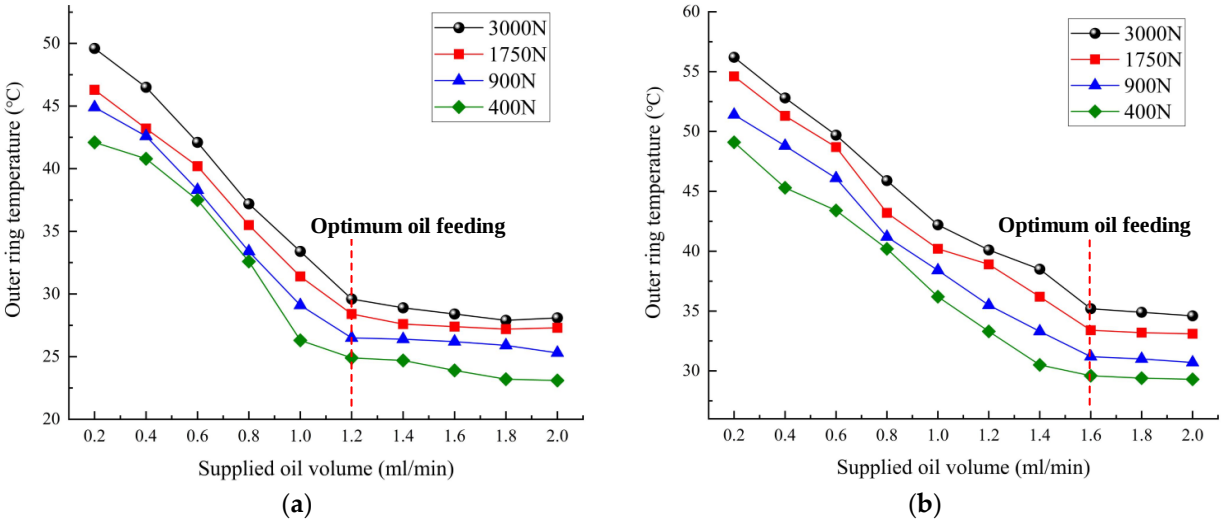

Figure 5. Temperature law of outer ring of full ceramic ball bearing under oil lubrication condition. (**a**) n = 5000 r/min, (**b**) n = 10,000 r/min.

According to the test data in Figure 5, with the increase of oil supply, the temperature rise of the outer ring gradually decreased. When the oil supply was lower than the optimal range, the temperature rise decreased obviously with the increase of oil supply. This is because, in the state of lack of oil lubrication, the lubrication effect of bearings is not good. The running state was mixed friction, and dry friction in some areas led to a significant rise in temperature. As the oil supply continued to increase, the lubrication state improved, and the temperature rise of bearing outer ring decreased. When the optimum oil supply was in place, the full ceramic ball bearing was in a state of full-film lubrication, which had a great improvement effect on the temperature rise of the bearing. When the oil supply continued to increase and was greater than the optimal oil supply, a large amount of lubricating oil removed the temperature rise generated by the operation of the bearing and caused a cooling effect, so the temperature rise of the bearing outer ring continued to decrease. The temperature rise of outer ring increased with the increase of bearing speed; it also increased with the increase of radial load. This is because, with the increase of the radial load and speed, the contact stress and contact frequency in the contact micro-zone of the full ceramic ball bearing became larger, and the heat generated by friction increased. The heat gradually accumulated in the outer ring of the bearing, and the temperature of the outer ring rose correspondingly.

4. Theoretical Calculation and Analysis

4.1. Oil Lubrication Dynamics Model of the Full Ceramic Ball Bearing

4.1.1. Establishment of Coordinate System of the Full Ceramic Ball Bearing

In the operation process of full ceramic ball bearings, the ceramic ball has the most complex force and contact with the inner and outer rings and cage, thus resulting in friction and impact. In addition, under the action of oil–gas lubrication, the ceramic ball was also affected by hydraulic force, which caused the ceramic ball to have a more complicated motion state [27,28]. In order to accurately describe the motion characteristics and interaction forces of the internal parts of the full ceramic ball bearing, a coordinate system was established, as shown in Figure 6.

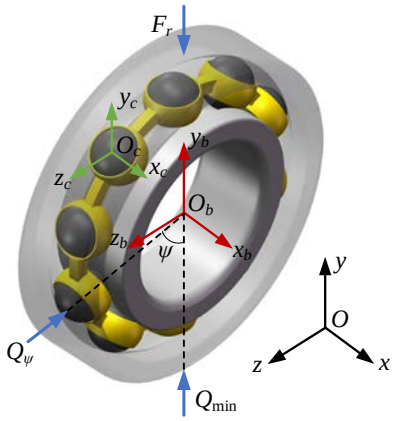

Figure 6. Coordinate system of deep groove ball bearing.

(I) The inertial coordinate system $Oxyz$ was established, with the bearing center O as the origin.
(II) The coordinate system $O_c x_c y_c z_c$ was established, with the spherical centroid O_c as the origin, y_C axis along the radial direction of the bearing, and ZC axis along the circumferential direction of the bearing.
(III) The inner circle centroid Ob was used as the origin to establish the coordinate system $O_b x_b y_b z_b$.

The force between the balls, rings, and cage is shown in Figure 7, in which the subscripts I and e represent the inner and outer rings, respectively, j represents the Jth ball, Q represents the normal contact force between the ball and the ring raceway, T_η and T_ξ are the drag forces on the contact surface between the ball and the ring raceway, Q_c represents the force of the cage pocket on the ball, and the angle between the cage pocket hole and the three directions of $O_p x_p y_p z_p$ in the coordinate system, βx, βy, βz. $P_{R\eta(\xi)}$, and $P_{S\eta(\xi)}$, are the rolling friction force and sliding friction force of the fluid at the entrance of the contact surface between the ball and cage pocket, respectively.

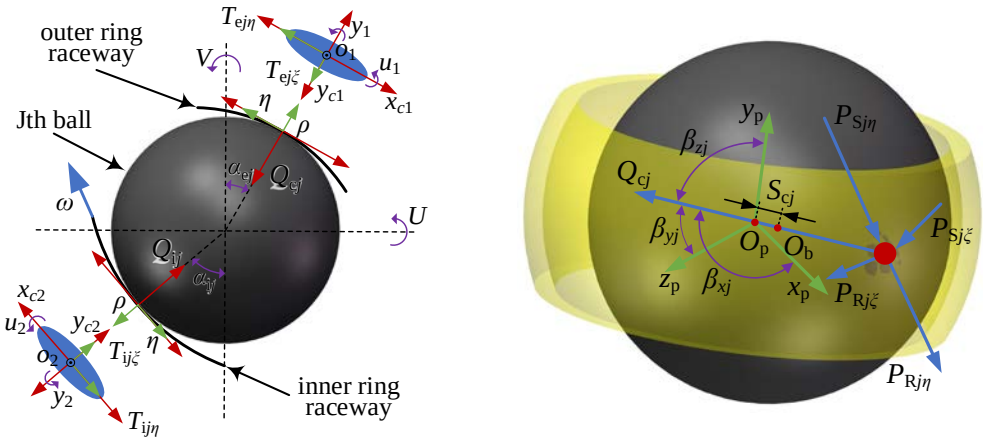

Figure 7. Mechanical model of full ceramic deep groove ball bearing. (**a**) Ball-ring contact force model, (**b**) Ball-cage contact force model.

4.1.2. Elastohydrodynamic Model of Full Ceramic Ball Bearing under Oil Lubrication

Under the action of oil–gas lubrication, each rolling body had two velocity directions of contact ellipse, i.e., the long and short axes, and the density and viscosity of lubrica-

tion medium changed along the direction of lubrication film thickness. Its steady-state generalized Reynolds lubrication equation can be written as follows:

$$\begin{cases} \frac{\partial}{\partial x_c}\left[\left(\frac{\rho}{\eta}\right)h^3\frac{\partial p}{\partial x_c}\right]+\frac{\partial}{\partial y_c}\left[\left(\frac{\rho}{\eta}\right)h^3\frac{\partial p}{\partial y_c}\right]=12U\frac{\partial(\rho_x^* h)}{\partial x_c}+12V\frac{\partial\left(\rho_y^* h\right)}{\partial y_c} \\ U=\frac{1}{2}(u_1+u_2) \\ V=\frac{1}{2}(v_1+v_2) \end{cases} \tag{1}$$

where h is the oil film thickness, p is oil film pressure distribution, and U and V are the entrainment velocity in x_c and y_c directions, respectively (the coiling speed in y_c direction is much higher than that in x_c direction), which is related to the actual contact speed between the inner and outer ring and the rolling bodies. ρ and η are density and viscosity coefficients, respectively, and $\rho_x{}^*$ and $\rho_y{}^*$ are the equivalent densities related to the equivalent viscosity of contact extrusion.

The lubrication film thickness h considering elastic deformation can be expressed as:

$$h=h_0+\frac{x_c^2}{2R_x}+\frac{y_c^2}{2R_y}+\delta(x_c,y_c) \tag{2}$$

where h_0 is the central film thickness of the elastic contact area, and R_x and R_y are the equivalent radius of curvature in the x_c and y_c directions, respectively. $\delta(x_c, y_c)$ is the elastic deformation in the contact region, and its expression is:

$$\delta(x_c,y_c)=\frac{2}{\pi E}\iint\limits_{\Omega}\frac{p(s,t)}{\sqrt{(x_c-s)^2+(y_c-t)^2}}\mathrm{d}s\mathrm{d}t \tag{3}$$

where E is the equivalent elastic model of two contact objects x.

4.1.3. Friction Torque

The rolling friction torque M_E generated when the ball rolls on the raceway was:

$$M_E=0.25D_{pw}\left[\left(1-\gamma_i^2\right)\sum_{j=1}^{z}\Phi_{ij}+\left(1-\gamma_e^2\right)\sum_{j=1}^{z}\Phi_{ej}\right]\beta_a \tag{4}$$

$$\gamma_{\mathrm{i}(e)}=D_{\mathrm{w}}\cos\alpha_{\mathrm{i}(e)}/D_{\mathrm{pw}} \tag{5}$$

where β_a is the elastic hysteresis coefficient. Φ can be calculated by referring to reference.

The friction torque M_{D} caused by differential sliding was:

$$M_{\mathrm{D}}=\frac{D_{\mathrm{pw}}}{2D_{\mathrm{w}}}\left[\left(1-\gamma_{\mathrm{i}}^2\right)\sum_{j=1}^{Z}M_{\mathrm{D}ij}+\left(1-\gamma_{\mathrm{e}}^2\right)\sum_{j=1}^{Z}M_{\mathrm{D}ej}\right]f_{\mathrm{s}} \tag{6}$$

where f_{s} is the sliding friction factor between the ball and the raceway. The friction moment M_{s} caused by the spin sliding of the ball was:

$$M_{\mathrm{s}}=\frac{3}{8}f_{\mathrm{s}}\left[\sum_{j=1}^{Z}\left(E_{\mathrm{w}}E_{\mathrm{i}}a_{\mathrm{i}}Q_{\mathrm{ij}}\sin\alpha_{ij}\right)+\sum_{j=1}^{Z}\left(E_{\mathrm{w}}E_{\mathrm{e}}a_{\mathrm{e}}Q_{\mathrm{ej}}\sin\alpha_{ej}\right)\right] \tag{7}$$

where E_{w} is the elastic modulus of the ball material. E_{i} and E_{e} are the elastic moduli of inner and outer ring materials, respectively. a_{i} and a_e are the long half axes of the contact ellipse of the inner and outer rings and the balls, respectively.

The friction torque M_{c} caused by the friction between the ball and the cage was:

$$M_{\mathrm{c}}=0.25D_{\mathrm{pw}}\left(1-\gamma^2\right)\times\sin\left(\alpha_0+\arctan\frac{D_w\sin\alpha_0}{2\gamma_1}\right)m_d\mu_c \tag{8}$$

where M_c is the cage mass and μ_c is the sliding friction coefficient between the ball and cage.

The friction torque M_l caused by the viscous resistance of lubricating oil in the running process of the bearing was:

$$M_l = 6.53\alpha^{-1}S_1D_{pw} \times \left\{ 2\sum_{j=1}^{Z}\left[\frac{h_{ij}+h_{ej}}{2}\left(\alpha_{ij}+\alpha_{ej}\right)\right]S_2 \right\}^{-1} \tag{9}$$

where S_1 is the sufficient lubrication coefficient, and the lubrication coefficient of oil film was taken. h is the oil film thickness in the center of the bearing contact area. S_2 is the side leakage coefficient of lubrication, and the value was 1 in the calculation.

In the process of rotational service, the total friction torque M of the bearing was:

$$M = M_E + M_D + M_s + M_c + M_l \tag{10}$$

4.1.4. Influence of Temperature Rise on Structural Parameters of the Full Ceramic Ball Bearing under Oil Lubrication Condition

Due to the inconsistent deformation of bearing inner and outer rings and ball under the condition of temperature rise change, the clearance of deep groove ball bearings will change, and the specific calculation formula is as follows:

$$\Delta p = \Delta p_i - \Delta p_o + 2\Delta p_r \tag{11}$$

$$C_r = C_0 + \Delta p \tag{12}$$

where Δp is the change of bearing clearance. Δp_o is the deformation of outer ring. Δp_i is the deformation of inner ring. Δp_r is the deformation amount of ceramic sphere. C_0 is the initial clearance of bearing. C_r is bearing clearance.

The deformation of bearing ring and cage affected by temperature change can be expressed as:

$$\Delta u = \Gamma_s D_c \Delta T \tag{13}$$

where Δu refers to the inner and outer diameters of bearing ring and cage. Γ is the expansion coefficient of the corresponding material. D_c represents the bearing inner and outer rings, as well as the cage's inner and outer diameter sizes. ΔT is the temperature difference.

4.1.5. Boundary Conditions

In order to ensure the convergence and accuracy of the contact elastohydrodynamic model of the full ceramic deep groove ball bearing, the value range of boundary coordinates was $x_{\text{in}} = 2a$, $x_{\text{out}} = 2a$, $y_{\text{in}} = 3.5b$, $y_{\text{out}} = 1.5b$. Thus, the x_c and y_c directions to solve the area was defined as: $\{(x_c,y_c) \mid -2a \le x_c \le 2a, -3.5b \le y_c \le 1.5b\}$ or less or less. In this paper, the region is divided into 50×50 grids in two directions.

Boundary conditions of Reynolds lubrication equation: boundary pressure was 0. The pressure of the whole bearing area was greater than or equal to 0. Considering the type of lubricating oil was isothermal solution, Thermo elastohydrodynamic lubrication(TEHL) method should be used to solve the problem. The pressure gradient in the oil film rupture zone was 0, as follows:

$$\begin{cases} p(x_{\text{in}},y_c) = p(x_{\text{out}},y_c) = 0 \\ p(x_c,y_{\text{in}}) = p(x_c,y_{\text{out}}) = 0 \\ p(x_c,y_c) \ge 0 (x_{\text{in}} < x_c < x_{\text{out}}, y_{\text{in}} < y_c < y_{\text{out}}) \\ \frac{\partial p(x_{\text{out}},y_c)}{\partial x_c} = \frac{\partial p(x_c,y_{\text{out}})}{\partial y_c} = 0 \end{cases} \tag{14}$$

4.2. Numerical Solution Process

Figure 8 shows the data coupling and solving process of the above equations.

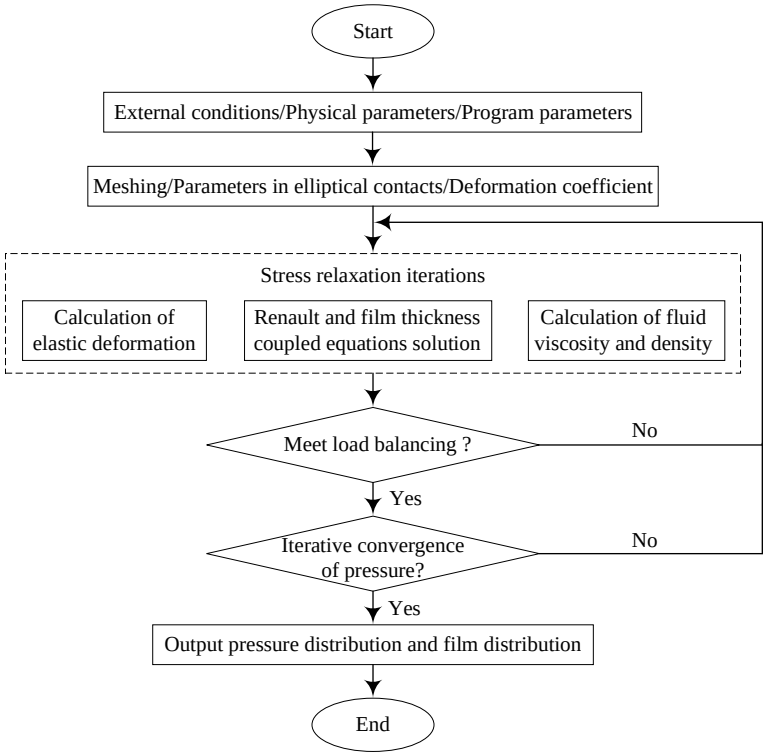

Figure 8. Flow chart of elastohydrodynamic coupling calculation of full ceramic ball bearings.

4.3. Calculation Results and Analysis

In 6208CE silicon nitride ceramic ball bearings, and combining the elastohydrodynamic lubrication equation shown in the Figure 2 flow calculation program, the test process to get the best oil for lubrication conditions, performing lubrication, and contact characteristics analysis were concluded, and the ceramic ball bearing lubrication under the condition of different speed and load of oil film thickness distribution of the simulation results are shown in Figure 9.

By comparing the simulation results in Figure 9a–f, it can be seen that the minimum liquid film thickness in the contact area of the rolling body decreased gradually with the increase of the angle ψ from the distance to the minimum stress point of the rolling body. This is because the squeezing effect of liquid film decreases with the increase of ψ. The minimum liquid film thickness of the rolling body at the same position increased with the increase of rotational speed and load. This was caused by the enhancement of dynamic pressure effect of oil film with the increase of rotational speed. Furthermore, the influence of rotational speed on the minimum liquid film thickness at different locations was similar, and the influence of rotational speed on the liquid film at different locations had no obvious change.

Under the condition of optimal oil supply lubrication for the full ceramic ball bearings, the pressure distribution of lubricating oil film of different rolling bodies under different rotational speeds and loads is shown in Figure 10.

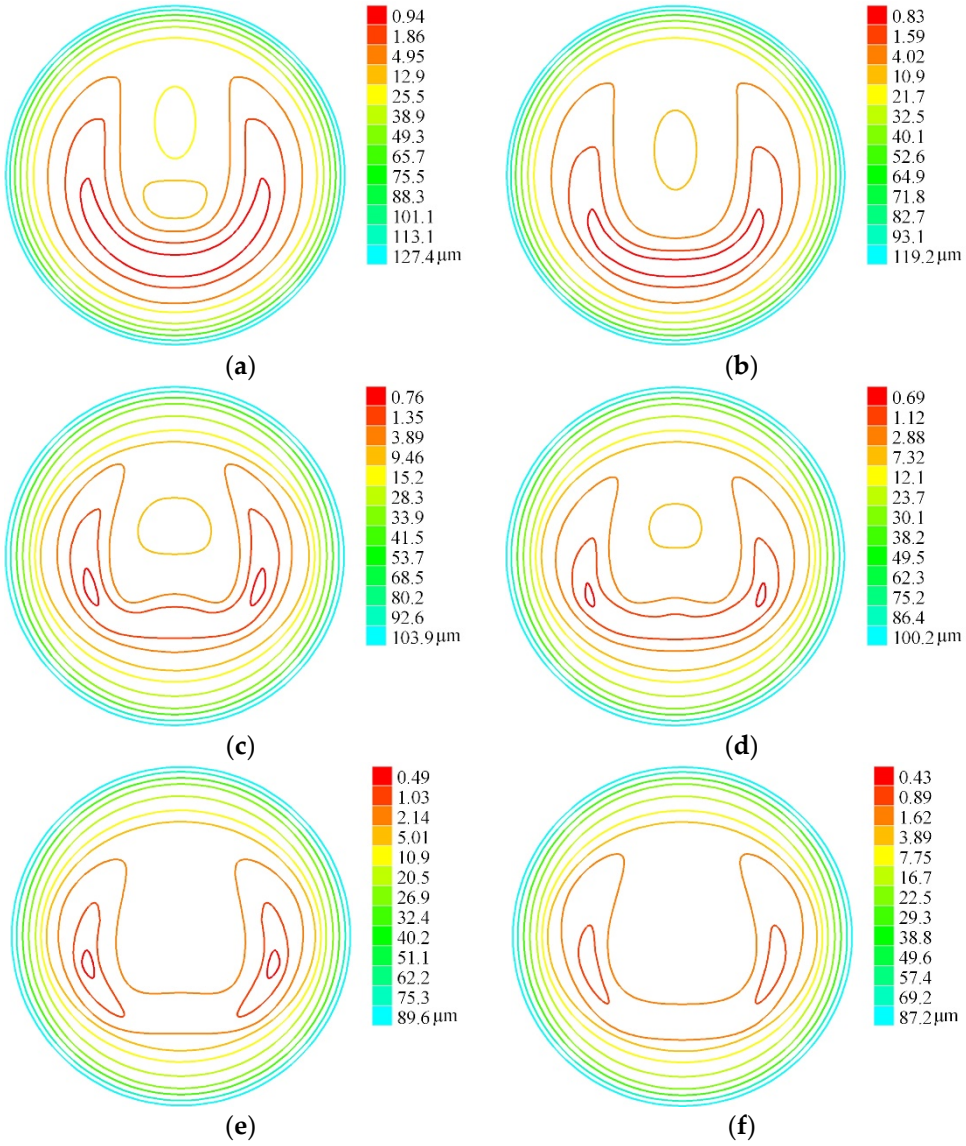

Figure 9. Oil film thickness distribution of ceramic ball bearings under different working conditions. (**a**) $\psi = 0°$, $F = 3000$ N, $n = 10{,}000$ r/min, (**b**) $\psi = 0°$, $F = 900$ N, $n = 5000$ r/min, (**c**) $\psi = 80°$, $F = 3000$ N, $n = 10{,}000$ r/min, (**d**) $\psi = 80°$, $F = 900$ N, $n = 5000$ r/min, (**e**) $\psi = 160°$, $F = 3000$ N, $n = 10{,}000$ r/min, (**f**) $\psi = 160°$, $F = 900$ N, $n = 5000$ r/min.

By comparing the simulation results of Figure 10a–f, it can be seen that the maximum pressure of the rolling body increased with the increment of ψ. This is because the maximum Hertz contact pressure of the rolling body increased with the increase of ψ. It can be seen from the figure that the maximum pressure of lubrication film decreased with the decrease of load contact pressure for different rolling bodies. The maximum oil film pressure corresponding to the rolling body at the same position increased with the increase of rotational speed and load. This was due to the enhanced dynamic pressure effect of oil film, caused by the increase of rotational speed. At the same speed, the angle between the rolling body and maximum stress position of the rolling body at different positions of the same bearing were larger, and the corresponding load was smaller, so the maximum oil film pressure caused by it also decreases correspondingly.

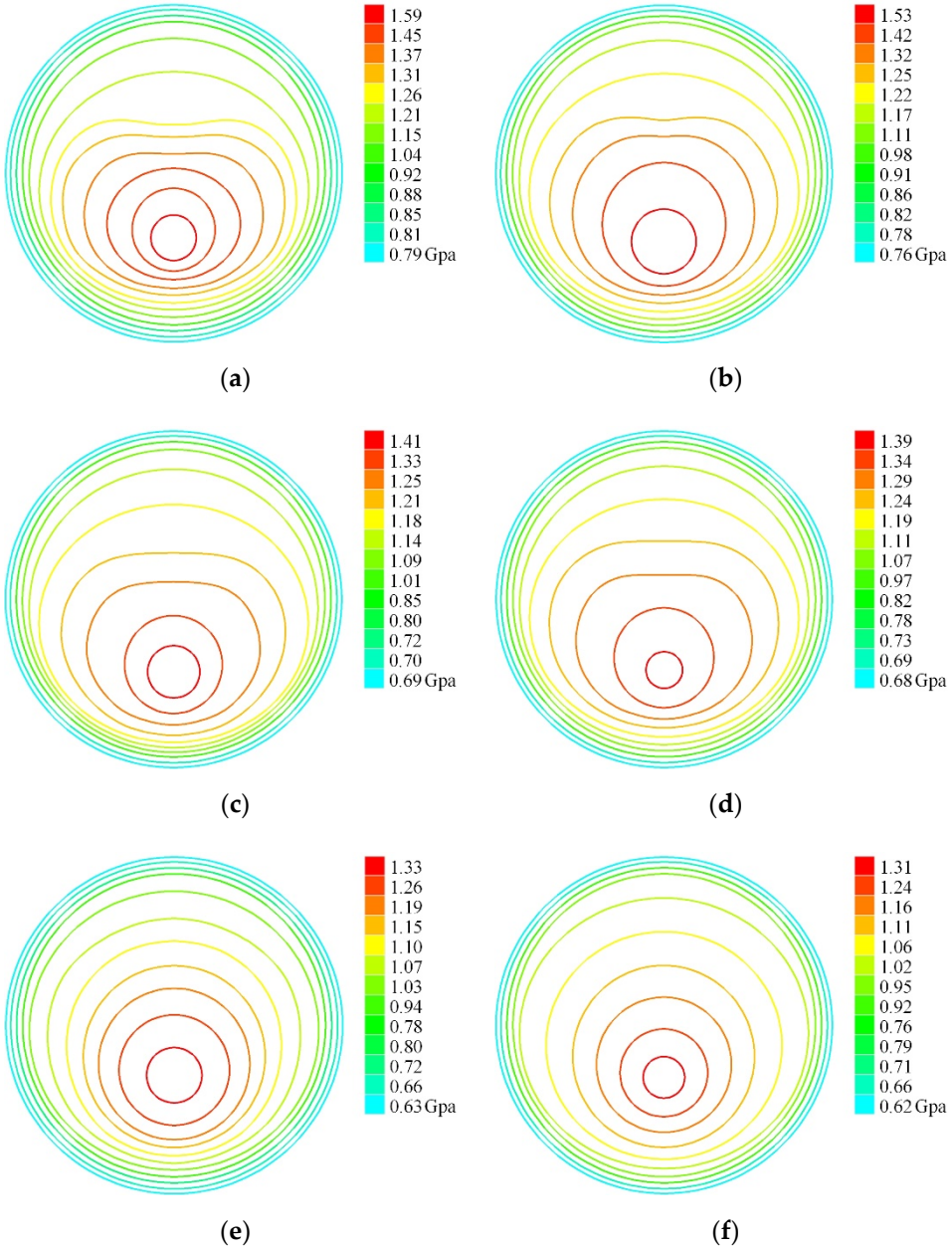

Figure 10. Oil film pressure distribution of ceramic ball bearings under different working conditions. (**a**) ψ = 0°, F = 3000N, n = 10,000 r/min, (**b**) ψ = 0°, F = 900 N, n = 5000 r/min, (**c**) ψ = 80°, F = 3000 N, n = 10,000 r/min, (**d**) ψ = 80°, F = 900 N, n = 5000 r/min, (**e**) ψ = 160°, F = 3000 N, n = 10,000 r/min, (**f**) ψ = 160°, F = 900 N, n = 5000 r/min.

By comparing the simulation and experimental results, it can be found that the thickness and pressure of the bearing oil film in the simulation model changed with the change of working conditions, and the change trend had a good consistency in the experimental results. In the case of large lubricating oil film thickness, the bearings showed excellent characteristics in the experiment. The reliability and correctness of the experimental data were verified.

5. Morphological Characteristics and Microstructure Properties of Contact Micro-Zone of Full Ceramic Ball Bearings under Oil Lubrication

5.1. Test Analysis of Full Ceramic Ball Bearings

The full ceramic ball bearings, tested under different lubrication conditions and working conditions, were tested and analyzed. Among them, the bearing in the figure below was tested under the condition of 900 N load, 5000 rpm, and 0.2 mL/min oil supply. After disassembling the tested bearing assembly, no obvious failure was found in the observation, as shown in Figure 11.

Figure 11. Removed silicon nitride full ceramic ball bearing and its components.

However, in Figure 11, the surface of the PVX cage side beam (the outer circular surface of the cage) showed obvious scratching and rubbing areas. According to the scratches, it can be judged that the surface of the outer ring and inner circle contact and collide when the bearing rotates. The reason for this phenomenon is that the cage was made of composite materials. According to the material properties in Tables 1 and 3, the thermal expansion coefficient of the cage was greater than that of silicon nitride. In the service process, due to the influence of temperature rise, the cage deformation was relatively large, and the cage was guided by the outer diameter. In this guidance mode, the coupling effects of temperature rise, load, and impact made the cage produce elliptic deformation, which then caused friction with the outer ring and inner circle, thus resulting in the cage's rub. In addition, PVX abrasive chips have certain lubricity, which helps to lubricate bearings in service conditions, to some extent.

5.2. Full Ceramic Ball Bearing Contact Area Surface and Surface Quality Testing

The contact area between the rolling body and the raceway was observed, as shown in Figure 12.

(**a**) (**b**)

Figure 12. Outer ring raceway and rolling bodies of full ceramic ball bearing after the test. (**a**) Bearing outer ring raceway, (**b**) Rolling bodies.

It can be seen from Figure 12 that there was no damage phenomenon on the surface of the contact area of the full ceramic ball bearing after the test. However, black film appeared in some areas of outer ring raceway and ball bearing surfaces. In order to further

reveal the chemical composition of the film, the mechanism of the film generation and its influence on the surface friction and wear quality of the bearing contact micro-zone were analyzed from the microscopic point of view. We performed non-destructive cutting of test bearing ring and cage. They were tested together with ceramic balls by SEM, XRD, and other instruments.

Hitachi S-4800 scanning electron microscope (SEM), which was made by Hitachi in Japan, was used to detect the raceway and black film covered area on ball surface after the test in Figure 12, as shown in Figures 13 and 14. As can be seen from scanning electron microscopy, the black film area was the covered area in Figures 13 and 14. This indicates that a thin film was formed on the surface of the contact micro-zone between the raceway and ball bearings under the coupling effects of temperature rise, heavy load, sliding effect, and cage collision. By comparing the pictures in Figures 12–14, it can be seen that both the macro- and micro-observation results show that the film formed on the surface of outer ring raceway had a better and more significant effect. Meanwhile, observe the removed bearing inner ring in Figure 11—the black film was not visible on its raceway surface.

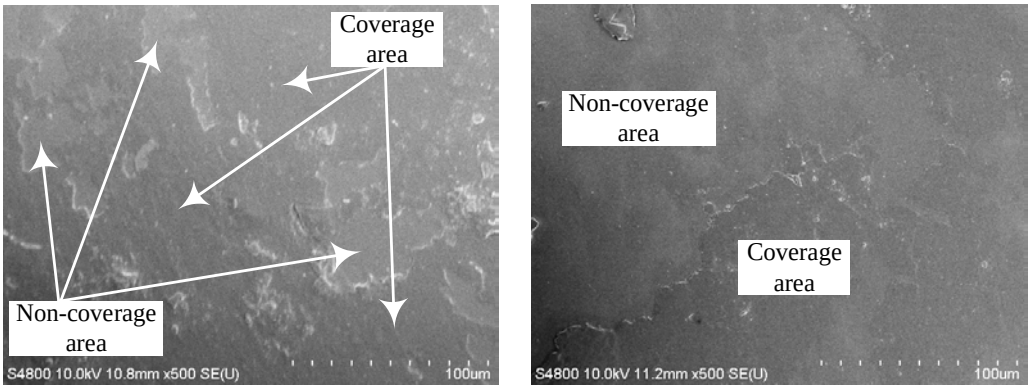

(**a**) (**b**)

Figure 13. SEM imaging of full ceramic ball bearing after the test. (**a**) Measuring point 1, (**b**) Measuring point 2.

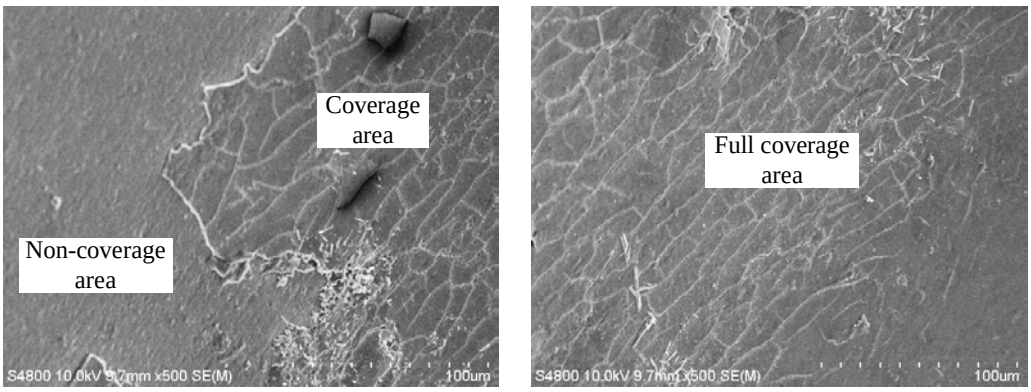

(**a**) (**b**)

Figure 14. SEM imaging of outer raceway of full ceramic ball bearing after the test. (**a**) Measuring point 1, (**b**) Measuring point 2.

The preliminary analysis of the reasons for the above phenomenon was that, when the full ceramic ball bearing ran in oil lubrication conditions, the debris on the outer ring of the cage and surface of the pockets were involved in the bearing contact micro area under the action of bearing rotation.

5.3. Chemical Composition and Qualitative Analysis of Surface Layer of Bearing Contact Area

The black film and cage on the outer racing surface of ceramic ball bearing were analyzed by Raman spectroscopy. In order to ensure the accuracy of the test, the components of the cage and raceway surface film were measured and analyzed twice, and the test results are shown in Figure 15.

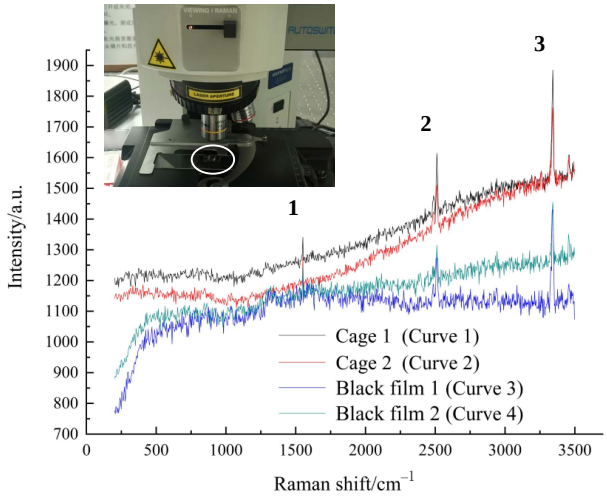

Figure 15. Raman spectra peaks of black film between cage and raceway after the test. 1–3. correspond to 3 characteristic peaks, respectively.

By comparing the four groups of measured curves in the figure, it can be seen that the spectral distribution trend of the film on the surface of the bearing cage and raceway were different after the test, that is, the 1/2 distribution trend of the curve is different from the 3/4 distribution trend of the curve. However, by comparing the three characteristic peaks of the four curves, it was found that the Raman wavelengths of the characteristic scattering peaks were almost the same. This indicates that the crystal interface between the cage and raceway surface film material was basically the same; we can preliminarily judge that the chemical compositions of the two groups of substances were similar.

XRD analysis was carried out on the powder of the outer ring raceway of the bearing and film layer on the surface of the ball and cage powder. The test results were shown in Figure 16.

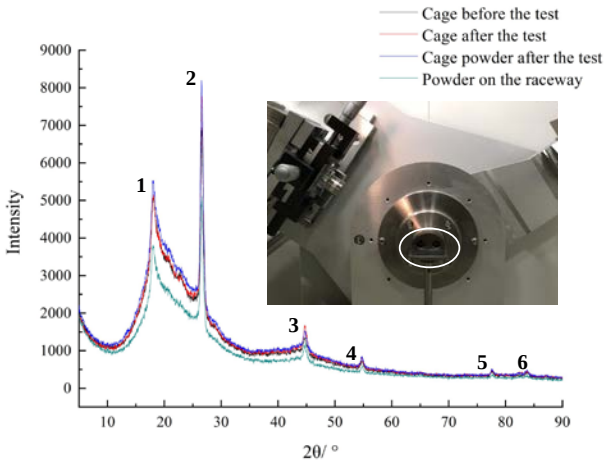

Figure 16. XRD spectrogram of cage and raceway black film. 1–6. correspond to 6 characteristic peaks, respectively.

The XRD results show that the phase diffraction peaks of the bearing cage and raceway film were basically the same before and after the test. Combined with the above analysis, it was preliminarily shown that PVX did not generate new substances by chemical reaction with the medium in the environment under the service conditions of extreme low variable temperature conditions. In Figure 15, the reason the distribution trend of curve 1/2 was different from that of curve 3/4 was that the film components formed by the retener powder under rolling action contain a very small amount of worn silicon nitride and sintering agent materials.

By comparing the above analysis results, it can be inferred that the powder formed by the cage under the action of physical conditions became the lubricating medium of the full ceramic ball bearing oil, which played a promoting role in the service of full ceramic ball bearings.

6. Conclusions

(1) In the service process of full ceramic ball bearing oil lubrication, there is an optimal oil supply. Under the action of the optimal oil supply lubrication, full-film lubrication can be achieved, and the bearing exhibits the optimal characteristics of friction, vibration, temperature rise, and so on. Compared with the load, the speed of the bearing has a decisive influence on the optimal oil supply. In this paper, it was found that the optimal oil supply of 6208CE silicon nitride full ceramic ball bearings was about 1.2 mL/min when the rotational speed was 5000 rpm. When the speed was 10,000 rpm, the optimal oil supply was about 1.6 mL/min.

(2) In the service process of full ceramic ball bearings, when the oil supply was less than the optimal oil supply, the full ceramic ball bearings were in the state of lacking oil lubrication, and the oil–solid mixed lubrication in the contact micro-zone led to the friction, vibration, and temperature rise of the bearings. When the oil supply was greater than the optimal oil supply, the viscous resistance generated by too much lubricating oil increased the friction and vibration of the bearing, but the friction and vibration were smaller than those in the state of poor oil lubrication. When the oil supply was too much, a large amount of lubricating oil reduced the temperature rise generated by the bearing, thus playing the role of lubrication and cooling, so the temperature rise of the bearing outer ring continued to decrease.

(3) When the rotational speed and load of the full ceramic ball bearing were constant, the extrusion effect and Hertz contact pressure increased gradually with the increase of the angle ψ from the minimum stress point of the rolling body, and the minimum oil film thickness and oil film pressure in the contact area of the rolling body decreased. When the speed and load of the bearing increased, the minimum oil film thickness and oil film pressure of the rolling body at the same position increased with the increase of the speed and load of the bearing, due to the influence of the dynamic pressure effect of the lubricating oil film.

(4) The full ceramic ball bearing can run under the above oil lubrication, as well as high speed and heavy load conditions. Key components, including ceramic ball, ceramic ring, and retainer, did not fail after detection. However, under the action of high contact stress, a film will be formed in the outer ring raceway of the bearing, which does not affect the service performance of the bearing. If the cage material is kept within the lubrication characteristics, the film has a certain promotion effect on the service of the bearing.

Author Contributions: Data curation, Z.B.; resources, Y.W.; software, Z.X., J.T. and L.G.; writing—original draft, J.Y. (Jinmei Yao); writing—review and editing, J.Y. (Jiaxing Yang) and J.S. All authors have read and agreed to the published version of the manuscript.

Funding: The authors acknowledge the collective support granted by the National Natural Science Foundation of China (grant No. 52105196), Department of Science and Technology of Liaoning Province (grant No. 2020-BS-159), and Young and Middle-aged Innovation Team of Shenyang (grant No. RC210343).

Data Availability Statement: Not applicable.

Conflicts of Interest: The authors declare no conflict of interest.

References

1. Yao, J.; Wu, Y.; Sun, J.; Xu, Y.; Wang, H.; Zhou, P. Research on the metamorphic layer of silicon nitride ceramic under high temperature based on molecular dynamics. *Int. J. Adv. Manuf. Technol.* **2020**, *109*, 1249–1260. [CrossRef]
2. Sun, J.; Wu, Y.; Zhou, P.; Li, S.; Zhang, L.; Zhang, K. Simulation and experimental research on Si3N4 ceramic grinding based on different diamond grains. *Adv. Mech. Eng.* **2017**, *9*, 9–14. [CrossRef]
3. Han, X.X.; Xu, C.H.; Jin, H.; Xie, W.H.; Meng, S.H. An experimental study of ultra-high temperature ceramics under tension subject to an environment with elevated temperature, mechanical stress and oxygen. *Sci. China Technol. Sci.* **2019**, *62*, 1349–1356. [CrossRef]
4. Sun, J.; Yang, J.X.; Yao, J.M.; Tian, J.X.; Xia, Z.X.; Yan, H.P.; Gao, L.F.; Li, S.H.; Bao, Z.G. The effect of lubricant viscosity on the performance of full ceramic ball bearings. *Mater. Res. Express* **2022**, *9*, 015201. [CrossRef]
5. Meyer, L.D.; Ahlgren, F.F.; Weichbrodt, B. An Analytic Model for Ball Bearing Vibrations to Predict Vibration Response to Distributed Defects. *J. Mech. Des.* **1980**, *102*, 205–210. [CrossRef]
6. Lynagh, N.; Rahnejat, H.; Ebrahimi, M.; Aini, R. Bearing induced vibration in precision high speed routing spindles. *Int. J. Mach. Tools Manuf.* **2000**, *40*, 561–577. [CrossRef]
7. Alfares, M.; Saleem, O.; Majeed, M. Analytical study of thermal variation impact on dynamics of a spindle bearing system. *Proc. Inst. Mech. Eng. Part K J. Multi-Body Dyn.* **2019**, *233*, 871–898. [CrossRef]
8. Jalali-Vahid, D.; Gohar, R.; Jin, Z.M.; Rahnejat, H. Comparison between experiments and numerical solutions for isothermal elastohydrodynamic point contacts. *J. Phys. D Appl. Phys. A Europhys. J.* **1998**, *31*, 2725. [CrossRef]
9. Hamrock, B.J.; Dowson, D. Isothermal Elastohydrodynamic Lubrication of Point Contacts: Part 1—Theoretical Formulation. *J. Lubr. Technol.* **1976**, *98*, 223–228. [CrossRef]
10. Ioannides, E.; Harris, T.A. A New Fatigue Life Model for Rolling Bearings. *J. Tribol.* **1985**, *107*, 367–377. [CrossRef]
11. Zhu, W.B.; Zhang, X.B.; Lu, Y.S.; Wang, D.L. Numerical Study on lubrication Performance of ball bearings. *J. Propuls. Technol.* **2019**, *4*, 892–901.
12. Nagare, P.N.; Kudal, H.N. Tribological Failure Analysis and Suitability of Grease Lubrication for Sugarcane Crushing Mill Journal Bearings. *J. Fail. Anal. Prev.* **2018**, *18*, 1311–1319. [CrossRef]
13. Lu, L.M.; Lu, J.F.; Li, Z.H. Lubrication Characteristics of roller bearing under Cyclic Impact Load. *Lubr. Eng.* **2021**, *12*, 78–85.
14. Kang, J.; Lu, Y.; Zhang, Y.; Liu, C.; Li, S.; Mueller, N. Investigation on the skidding dynamic response of rolling bearing with local defect under elastohydrodynamic lubrication. *Mech. Ind.* **2019**, *20*, 615. [CrossRef]
15. Antonio, G.; Linares, F.; Arias, M. Numerical Investigations of the Lubrication Conditions in Hydrodynamic Bearings with Shaft Misalignment Effect. *Ing. Investig. Y Tecnol.* **2013**, *14*, 89–98.
16. Cho, I. The influence of boundary conditions on the lubrication characteristics of a journal bearing for reciprocating compressors. *J. Mech. Sci. Technol.* **2015**, *29*, 751–758. [CrossRef]
17. Biswas, N.; Chakraborti, P.; Belkar, S. An analytical and experimental approach for pressure distribution analysis of a particular lobe and plain bearing performance keeping in view of all impeding varying parameters associating with fixed lubrication SAE20W40. *J. Mech. Sci. Technol.* **2016**, *30*, 2187–2193. [CrossRef]
18. Dmitrichenko, N.F.; Milanenko, A.A.; Hluhonets, A.A.; Minyaylo, K.N. Method of Forecasting Durability of Bearings Rolling and Optimal Choice of Lubricants under Conditions of Flood Lubrication and Oil Starvation. *Treniei Iznos* **2017**, *38*, 114–120.
19. Brizmer, A.; Gabelli, C.; Vieillard, G.E.; Morales, E. An Experimental and Theoretical Study of Hybrid Bearing Micropitting Performance under Reduced Lubrication. *Tribol. Trans.* **2015**, *58*, 829–835. [CrossRef]
20. Li, K.; Chen, Z.X.; Liu, P.P.; Li, G.; Ding, M.; Li, Z.X. Characterization and performance analysis of 3D reconstruction of oil-lubricated Si_3N_4–GCr15/GCr15–GCr15 friction and wear surface. *J. Therm. Anal. Calorim.* **2020**, *144*, 2127–2143. [CrossRef]
21. Xiang, G.; Wang, C.; Wang, Y.J.; Han, Y.F.; Wang, J.X.; Lv, Z. Dynamic Mixed Lubrication Investigation of Water-Lubricated Bearing With Unbalanced Rotor During Start-Up. *Tribol. Trans.* **2021**, *64*, 764–776. [CrossRef]
22. Ma, S.; Zhang, X.; Yan, K.; Zhu, Y.; Hong, J. A Study on Bearing Dynamic Features under the Condition of Multiball–Cage Collision. *Lubricants* **2022**, *10*, 9. [CrossRef]
23. Sun, X.; Zhang, W.H.; Tian, H. Theoretical analysis of cylindrical roller bearing with flexible rings mounted in groove elastic support:Papers. *J. Adv. Mech. Des. Syst. Manuf.* **2020**, *14*, JAMDSM0102. [CrossRef]
24. Zheng, Y.; Zhao, S. Research on the Performance of radial sliding Bearing with sliding Surface considering cavitation pressure. *Lubr. Eng.* **2017**, *7*, 54–59.
25. Du, F.M.; Chen, C.D.; Zhang, K.G. Fluid Characteristics Analysis of the Lubricating Oil Film and the Wear Experiment Investigation of the Sliding Bearing. *Coatings* **2022**, *12*, 67. [CrossRef]

26. Shetty, P.; Meijer, R.J.; Lugt, P.M. An Evaporation Model for Base Oil from Grease-Lubricated Rolling Bearings including Breathing. *Tribol. Trans.* **2021**, *64*, 891–902. [CrossRef]
27. Zhang, Y.; Luo, Y.; Ni, S.; Wu, R.; Zhang, Z.Q. High speed characteristics of lubricating oil film of heavy hydrostatic bearing with micro inclined plane. *J. Jilin Univ.* **2021**, *2*, 450–457.
28. Xu, G.; Geng, H.P.; Zhou, J.; Yu, L.; Yang, L.; Lu, J.M. Research on the Static and Dynamic Characteristics of Misaligned Journal Bearing Considering the Turbulent and Thermohydrodynamic Effects. *J. Tribol.* **2015**, *137*, 024504. [CrossRef]